



OPEN ACCESS

EDITED BY

Liang Xiao,
Dalian Maritime University, China

REVIEWED BY

Jiu Haifeng,
Harbin University of Commerce, China
Pengfei Xu,
Hohai University, China
Zaopeng Dong,
Wuhan University of Technology, China

*CORRESPONDENCE

Pengyun Chen
✉ chenpengyun@nuc.edu.cn
Ying Liu
✉ liuying@hsddyxy.com
Lei Zhang
✉ zhanglei103@hrbeu.edu.cn

RECEIVED 07 April 2023

ACCEPTED 08 May 2023

PUBLISHED 19 May 2023

CITATION

Chen P, Liu Y, Chen X, Ma T and Zhang L
(2023) Underwater terrain positioning
method based on Markov random field for
unmanned underwater vehicles.
Front. Mar. Sci. 10:1201716.
doi: 10.3389/fmars.2023.1201716

COPYRIGHT

© 2023 Chen, Liu, Chen, Ma and Zhang. This
is an open-access article distributed under
the terms of the [Creative Commons
Attribution License \(CC BY\)](https://creativecommons.org/licenses/by/4.0/). The use,
distribution or reproduction in other
forums is permitted, provided the original
author(s) and the copyright owner(s) are
credited and that the original publication in
this journal is cited, in accordance with
accepted academic practice. No use,
distribution or reproduction is permitted
which does not comply with these terms.

Underwater terrain positioning method based on Markov random field for unmanned underwater vehicles

Pengyun Chen^{1*}, Ying Liu^{2*}, Xiaolong Chen³, Teng Ma⁴
and Lei Zhang^{4*}

¹School of Aerospace Engineering, North University of China, Taiyuan, China, ²College of Oriental Languages, Harbin Normal University, Harbin, China, ³China Ship Development and Design Center, Wuhan, China, ⁴Science and Technology on Underwater Vehicle Laboratory, Harbin Engineering University, Harbin, China

Underwater terrain-matching navigation technologies have become a popular topic for the high-precision positioning and navigation of autonomous underwater vehicles. This paper proposes an underwater terrain-matching positioning method based on a Markov random field model, which is based on real-time terrain data obtained using a multi-beam echo sounder. It focuses on the strong correlation between adjacent terrain data, which can improve terrain adaptability and matching accuracy. Playback simulation tests were conducted based on actual sea trial data, and the results showed that the proposed method has good positioning performance, which can correct the cumulative errors of inertial navigation systems. The results demonstrated the usability of the proposed method for positioning correction in underwater engineering applications.

KEYWORDS

unmanned underwater vehicles, Markov random field (MRF), multi-beam sounding data, terrain-aided navigation, semi-physical simulation

1 Introduction

Underwater terrain matching navigation (UTMN) technology has become a popular research topic in developing an error correction method for inertial navigation systems (INSs) for the underwater sailing of unmanned underwater vehicles (UUVs) (Huang et al., 2019; Zhang et al., 2020a).

Several terrain-matching methods are available. Terrain contour matching (TERCOM) and Sandia inertial terrain-aided navigation (SITAN) have been successfully used for aircraft navigation (Feng, 2004). Unlike terrain matching methods applied in aircrafts, UTMN has long been impeded by high-precision underwater terrain data. With the wide use of underwater multi-beam terrain measurement technology, it has become possible to create underwater digital terrain maps (DTMs) with high accuracy, enabling an in-depth study of UTMN (Hagen et al., 2012; Li et al., 2018).

In contrast to single-beam (Zhang et al., 2020b) and multi-line (Salavasidis et al., 2019) measurement methods, hundreds or even thousands of sounding data can be obtained simultaneously using a multi-beam echo sounder (MBES), where the measured terrain is the surface terrain, which can provide abundant sounding data as a solid foundation for UTMN (Jalving et al., 2004). Generally, UTMN methods based on MBES can be divided into two categories: continuous terrain filtering methods (CTFMs) and underwater terrain positioning methods (UTPMs). CTFMs include the Kalman filter (Zhou and Zheng, 2012), particle filter (Zhao et al., 2015; Teixeira et al., 2017), and point-mass filter (Bergman and Ljung, 1997), which were developed using SITAN. Thus, CTFMs have been widely researched to achieve good matching performance and continuous navigation and positioning correction. However, continuous navigation and positioning correction are dependent on the continuous measurement of the terrain, and the measurement sensor must operate continuously, which consumes considerable amount of power. Owing to the poor energy reserves of UUVs, CTFMs based on MBES are not suitable for engineering applications unless the battery field has a major technological breakthrough (Ma et al., 2020). Thus, CTFMs typically use low-power sensors, such as the Doppler velocity log (DVL) and acoustic altimeter, for water depth measurements (Salavasidis et al., 2021; Jiang et al., 2022). Compared with CTFMs, UTPMs were developed using TERCOM, which only requires multiple terrain-measured profiles (ping), which is relatively more advantageous. Traditional UTPM algorithms are based on terrain correlation estimations such as least-squares (Chen et al., 2015a), maximum likelihood (Chen et al., 2012; Peng et al., 2016), and Bayesian estimation (Chen et al., 2019a). Theoretically, the terrain correlation estimations are affected by “error averaging,” which can reduce the positioning accuracy in terrain flat areas. Existing methods assume that depth data are independent of each other, and the correlation of adjacent terrain data is not considered. Thus, terrain features are not fully utilized in existing methods.

The Markov random field (MRF) is an effective mathematical model for describing the grayscale dependence between image pixels and has been successfully applied in image matching (Shekhovtsov et al., 2008). The gridded DTM has properties similar to those of a grayscale image (Ma, 2019), and neighboring terrain data also have dependency relationships. Thus, the MRF model can also be used to describe terrain features. Considering the strong correlation between terrain data, this paper proposes a UTPM based on the MRF model. Simulation results show that the proposed method has excellent positioning accuracy and real-time performance, which are suitable for UUV underwater navigation.

2 Terrain positioning model

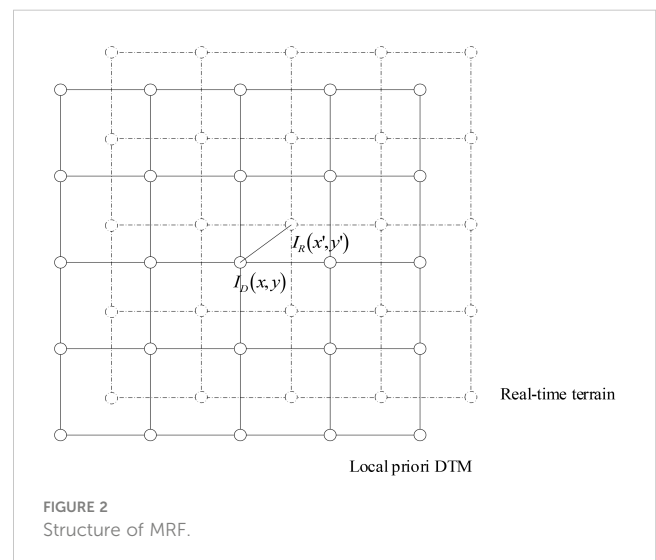
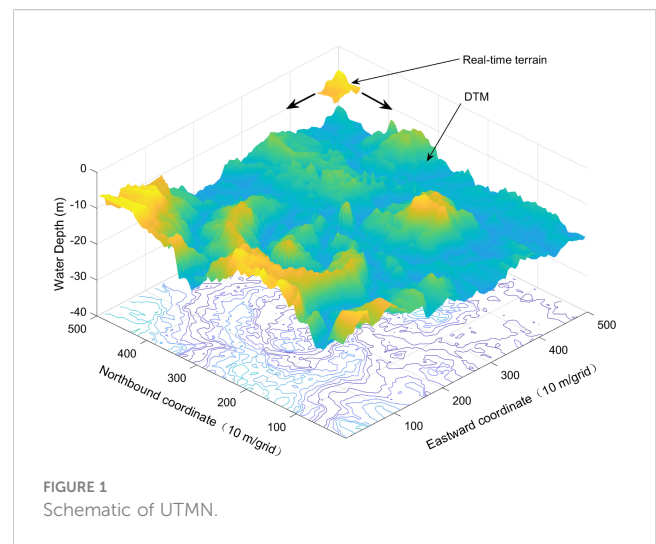
The UTPM, which differs from the traditional terrain height matching model, is presented as a terrain feature matching model in this paper. Therefore, the relationship between terrain data is considered. After filtering and gridding (Chen et al., 2015b; Chen et al., 2021), a terrain data matrix is obtained based on real-time multi-beam data, which have the same gridding space as the priori

DTM (Arashloo and Kittler, 2011). The structure of the MRF between the real-time terrain and the local priori DTM is shown in Figure 1.

In Figure 2, $I_D(x,y)$ and $I_R(x',y')$ are the depth data distributions of the local priori DTM and real-time terrain, respectively, and (x,y) and (x',y') are the coordinates of the terrain data in the local priori DTM and real-time terrain, respectively (Matthies and Okutomi, 1990; Xu and Chen, 2005). From Figure 2, the underwater terrain-positioning model can be expressed using Eq. (1):

$$I_D(x,y) = I_R(x',y') = I_R[x + d_x(x,y), y + d_y(x,y)] + e(x,y) \tag{1}$$

where $d_x(x,y)$ and $d_y(x,y)$ are the position deviations of the real-time terrain, and $e(x,y)$ is the measurement error. As shown in Eq. (1), the basic concept of MRF-based UTPM is to calculate the values of $d_x(x,y)$ and $d_y(x,y)$. To establish an MRF-based underwater terrain positioning model, the following assumptions are introduced in this study:



Assumption 1: The INS cumulative error obtained within a short time can be ignored, which is significantly more accurate than the multi-beam data error. Therefore, we assume that there is no relative position error in the terrain measurement during UTPM.

Assumption 2: Because of the continuity of the underwater terrain, there are strong correlations between adjacent terrain data. Thus, the terrain data have a probability dependency, which can be expressed by the MRF model.

Assumption 3: After grid processing, the locations of the terrain data are fixed in the real-time data and local priori DTM; d_x and d_y are independent constants.

Assumption 4: The measurement error of MBES is not Gaussian, however, the noise mean is much smaller than the water depth, Thus, the measurement error can be can be approximately considered as Gaussian white noise.

3 MRF-based UTPM algorithm

3.1 Gibbs distribution of terrain data

Based on the above assumptions and the maximum a posteriori estimation principle, when the distributions of the local priori DTM and real-time terrain are known, the MRF-based UTPM problem can be described as determining the deviation (d_x and d_y) of the real-time terrain data from the local priori DTM, which maximizes the posterior probability distribution $P(I_R|I_D)$ according to the Bayesian function:

$$P(I_R|I_D) = \frac{P(I_D|I_R)P(I_R)}{P(I_D)} \tag{2}$$

$$= \frac{P(I_D-I_R)P(I_R)}{P(I_D)} \propto P(I_D - I_R)P(I_R)$$

As shown in Eq. (2), $P(I_R|I_D)$ adheres to the MRF distribution, and the estimated values of d_x and d_y are related to the probability distributions of the measurement error $P(e)$ and the real-time terrain $P(I_R)$. Thus, the aim of MRF-based UTPM is to determine $P(e)$ and $P(I_R)$. According to the Hammersley–Clifford theorem (Chen et al., 2019b) and Assumption 2, $P(I_R)$ can be expressed by the Gibbs function:

$$P(I_R) = Z^{-1} \exp \left[-\frac{1}{T} U(I_R) \right] \tag{3}$$

where Z is a normalized constant, and T is a temperature constant. $U(I_R)$ is an energy function related to I_R . Based on the Gibbs distribution model proposed by Geman (Geman and Geman, 1984), $U(I_R)$ can be defined using Eq. (4).

$$U(I_R) = \sum_{x,y \in W} \sum_{m,n=-1}^1 [I_R(x+d_x, y+d_y) - I_R(x+m+d_x, y+n+d_y)]^2 \tag{4}$$

$$|m| + |n| = 1$$

where W is a matching window, and m and n are used to describe the four neighborhoods of the Gibbs distribution.

3.2 Position deviation estimation

Let W_R and W_D be matching windows of the same size, selected in the real-time terrain and local *a priori* DTM. From Eq. (1) and Assumption 3,

$$e(x, y) = I_D(x, y) - I_R[x + d_x, y + d_y] \tag{5}$$

Using the Taylor expansion $I_R[x+d_x, y+d_y]$ at $(x+d_x, y+d_y)$, Eq. (5) can be expressed as

$$e(x, y) = I_D(x, y) - I_R(x, y) - d_x \frac{\partial I_R}{\partial x} - d_y \frac{\partial I_R}{\partial y} \tag{6}$$

Assuming $d_y=0$, and considering the positional deviation in the x direction, let $e(x) \sim N[0, \sigma_n^2]$ be based on Assumption 4 and Eq. (6) can be written as a function of d_x .

$$e_x(x, y) = I_D(x, y) - I_R(x, y) - d_x \frac{\partial I_R}{\partial x} \tag{7}$$

and

$$p(e_x) = \prod_{x,y \in W} p[e_x(x, y), (x, y) \in W] \tag{8}$$

$$= \prod_{x,y \in W} \frac{1}{\sqrt{2\pi}\sigma_n} \exp \left[-\sum_{x,y \in W} \frac{[e_x(x, y)]^2}{2\sigma_n} \right]$$

Let $K_x = \prod_{x,y \in W} \sqrt{2\pi}\sigma_n$, $E(d_x) = \sum_{x,y \in W} \frac{[e_x(x, y)]^2}{2\sigma_n}$; based on Eqs. (2), (3), (4) and (8), the following equation is obtained:

$$P(I_R|I_D) \propto \frac{1}{K_x} \exp \{-[E(d_x) + U(I_R)]\} \tag{9}$$

In Eq. (9), K_x is independent of d_x . Therefore, the aim of the MRF-based UTPM is to determine a d_x value that minimizes $E(d_x) + U(I_R)$. The estimated value of d_x is given by Eq. (10).

$$\hat{d}_x = \arg \min \left\{ \sum_{x,y \in W} \frac{[e_x(x, y)]^2}{2\sigma_n} + \Phi(x, y) \right\} \tag{10}$$

Where

$$\Phi(x, y) = \sum_{x,y \in W} \sum_{m,n=-1}^1 [I_R(x+d_x, y) - I_R(x+m+d_x, y+n)]^2 \tag{11}$$

$$|m| + |n| = 1$$

Based on the same analysis, the value of d_y is given by Eq. (12).

$$\hat{d}_y = \arg \min \left\{ \sum_{x,y \in W} \frac{[e_y(x, y)]^2}{2\sigma_n} + \Psi(x, y) \right\} \tag{12}$$

$$\Psi(x, y) = \sum_{x,y \in W} \sum_{m,n=-1}^1 [I_R(x, y+d_y) - I_R(x+m, y+n+d_y)]^2 \tag{13}$$

$$|m| + |n| = 1$$

Therefore, the matching position results (x', y') are obtained as expressed in Eq. (14).

$$\hat{x}' = x + \hat{d}_x, \hat{y}' = y + \hat{d}_y \quad (14)$$

3.3 Matching process

The matching process is conducted as follows:

1. Inputting the real-time sounding data and the local priori DTM;
2. Filtering and gridding the real-time sounding data; let the real-time terrain have the same grid spacing as the local priori DTM;
3. Calculating the Gibbs distribution using Eq. (4);
4. Using Eq. (7), calculating $e_x(x, y)$ and $e_y(x, y)$;
5. Using Eqs. (10) and (12), calculating \hat{d}_x and \hat{d}_y ;
6. Using Eq. (14), calculating the matching position (x', y') ;
7. Outputting the calculation results to navigation.

The flowchart of the proposed method is shown in Figure 3.

In the proposed UTPM algorithm, terrain-matching positioning considers only the navigation deviation of the INS in

the east and north directions, and the angle and sky deviations can be ignored. However, depth offset cannot be ignored. The reasons are as follows (Nygren, 2005; Chen et al., 2019b; Salavasisidis et al., 2019):

1. The UTPM is an MBES, and the matching results are minimally affected by other sensor errors. The impact of systematic errors in attitude (including heading, pitch, and roll) on measurement data is virtually negligible in most terrain-aided navigation methods if adequate motion sensors are available.
2. Although the INS error is a combined effect of multiple error sources in the velocity and heading measurements, the drift in attitude is much smaller than the drift in the position estimates.
3. In addition, both the pressure sensor and altimeter provide accurate measurements to estimate the depth with an error of less than 0.01% of the operation depth.
4. Because of unknown tides and random waves, the depth offset cannot be disregarded. Therefore, it is necessary to eliminate the reference depth deviation while normalizing and establishing a terrain-matching surface.

4 Simulation and analysis

4.1 Simulation system

Simulation tests were conducted using an underwater semi-physical simulation system. The system center was a PC104 embedded computer. The structure of the simulation system is shown in Figure 4.

The simulation system comprised three parts: a monitoring computer, environment simulation computer, and PC104 embedded computer.

The monitoring computer was an actual AUV monitoring computer responsible for issuing task-level parameters and start-up instructions. Additionally, the "AUV" status information could be displayed. The environment simulation computer simulated the AUV movement in the marine environment and the sensors carried by the AUV. The PC104 embedded computer ran the AUV control system and had the same parameters as the master computer of the AUV. The difference was that the sensor information was the data packet sent by the environment simulation computer, and the actuator information was also sent to the environment simulation computer *via* Ethernet. The primary parameters of the PC104 computer are listed in Table 1.

Based on the simulation system, the simulation test was divided into two parts:

Test 1: Algorithm validation based on different terrain feature conditions to verify feasibility of the proposed algorithm.

Test 2: Playback simulation test using complete MBES survey line data to verify the applicability of the proposed algorithm in a real marine environment.

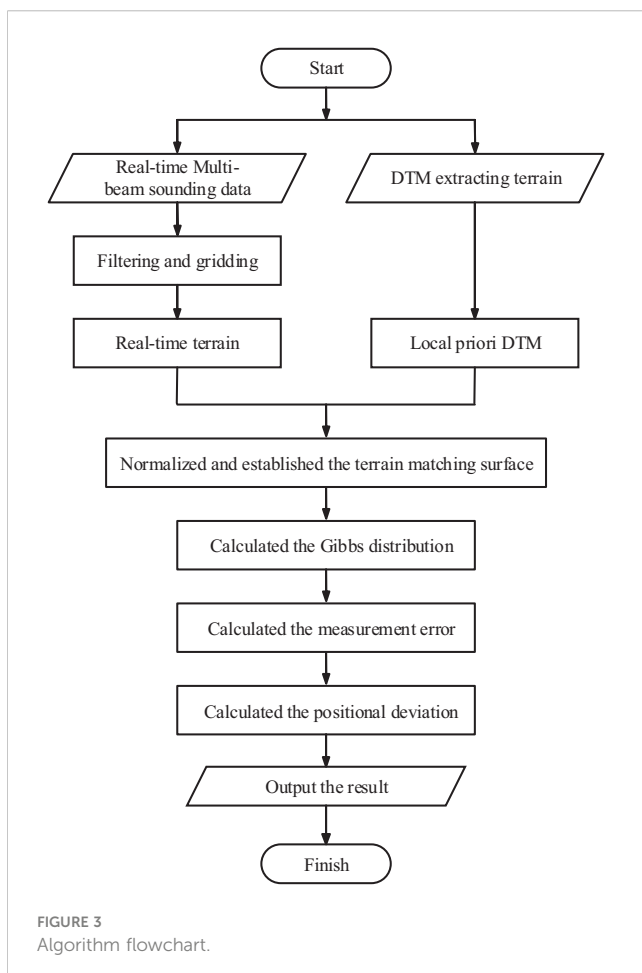


FIGURE 3
Algorithm flowchart.

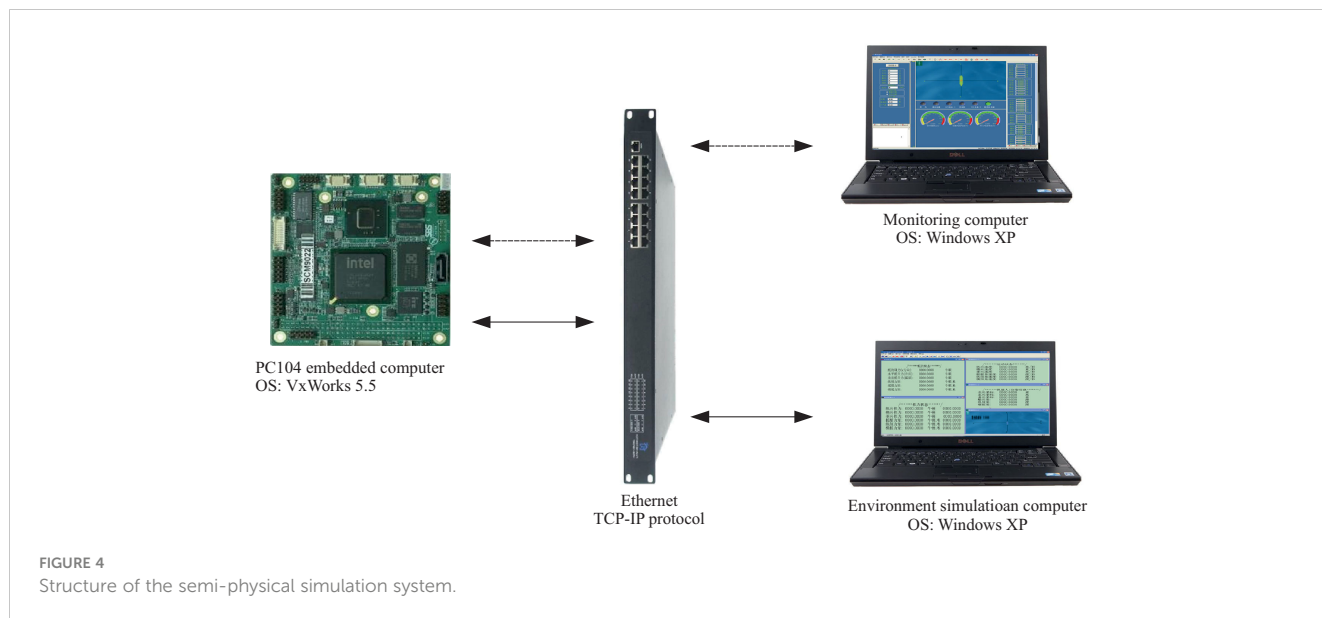


TABLE 1 Specifications of the PC104 computer.

Entry	Description
Brand (product model)	SBS(PMI2)
CPU	Intel Pentium M@2.0 GHz
Chipset	Intel85XGME/ICH4
Memory	256 MB
LAN	Ethernet Controller Integrated in ICH4
Operating System	VxWorks 5.5

4.2 Simulation data source

During the simulations, the DTM data source was measured using a GeoSwath Plus (GS+) during a sea trial (Figure 5). GS+ is a typical MBES based on the principle of phase interference (GeoAcoustics Limited, 2007), produced by Kongsberg GeoAcoustics Ltd., Great Yarmouth, UK. The hardware composition of GS+ is shown in Figure 5, and its main parameters are listed in Table 2.

The sea trial area (1000 m × 900 m), with a depth of 5–40 m, was located close to Qingdao (Figure 6). After the filtering and

gridding processes, a DTM with 1 m × 1m grid spacing was created, as shown in Figure 7.

The path indicated by the black line in Figure 7B is an independent survey line drawn using GS+, which can be used to simulate the MBES data. After the calculation of the terrain characteristics of the survey line that runs through the measured region, eight positioning areas were selected; the size of each area was 100 m × 100 m, and the center of the matching areas is shown in Figure 7B. To compare the richness of the terrain characteristics, the terrain entropies (Wang et al., 2007) of the selected positioning areas were calculated as shown in Table 3.

The raw file of the GS+ contains the navigation data of the measured terrain. The navigation data in the raw file are real-time kinematic (RTK) data, and the theoretical positioning accuracy that can be achieved is at the centimeter level. Therefore, real values of terrain positioning can be used through RTK (Yao et al., 2016). Based on the simulation system, the simulation test was divided into algorithm validation and playback simulation tests. An algorithm verification test was used to analyze the main factors affecting the positioning effect by comparing it with typical terrain positioning methods. A playback simulation test was conducted using sea trial data to verify the applicability of the proposed algorithm in an actual marine environment.

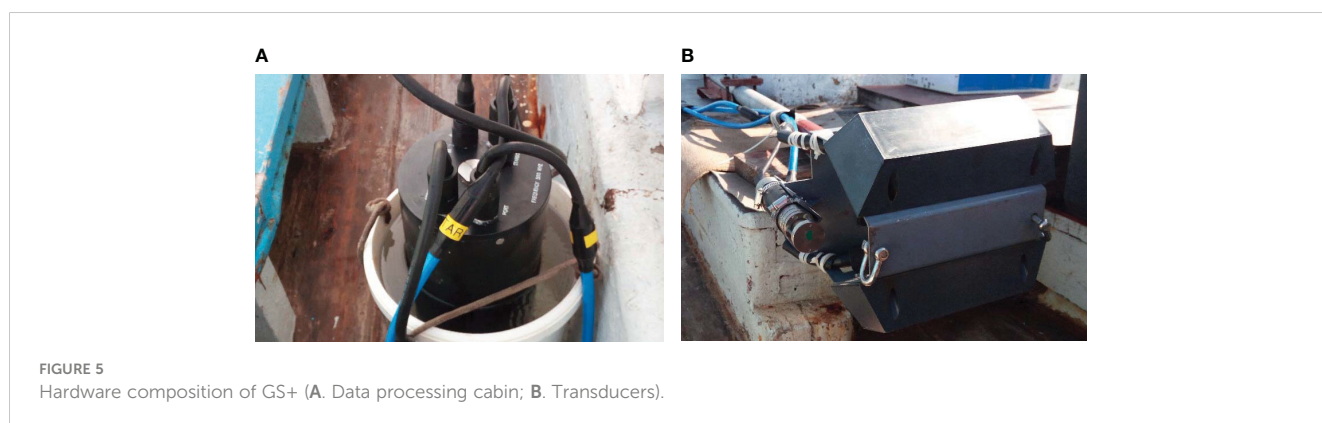


TABLE 2 Main parameters of GS+.

Parameter name	Value
Transducer size	5 cm×11 cm×6 cm
Working frequency of transducer	500 kHz
Maximum working depth	50 m
Maximum swath width	150 m
Maximum open angle of sector	150°
Maximum beam range	12×depth
Maximum beam number	>5000/ping
Maximum data update frequency	30 Hz

4.3 Algorithm validation

For algorithm validation, the real-time terrain was directly intercepted from an independent survey line. For comparison, other simulation tests were performed under same simulation conditions using the UTPM method based on maximum

likelihood estimate (MLE), which was proposed in reference (Chen et al., 2012). In this method, the maximum likelihood algorithm is used for correlation analysis of terrain features; for the influence from false peaks of likelihood function at flat bottom area, the Fisher criterion is introduced, and the false peaks are eliminated effectively, which can enhance the discrimination of terrain flat area. The following simulation tests were executed to verify the advantages of the proposed method and analyze the main factors affecting it. The following simulation tests were executed, and the simulation results were obtained based on the mean of the results of 200 simulation tests.

Simulation 1. After the filtering and gridding processes, the size of the real-time terrain was 40×30. By selecting different initial positioning errors (IPEs), the simulation results are shown in Figures 8, 9. The positioning accuracy of the MRF-based method is independent of the terrain entropy, indicating that the MRF-based method has good terrain adaptability. However, the MRF-based method is sensitive to IPEs, and the positioning error increases sharply with increasing IPE. When the IPE reached 30 m, the positioning results were divergent; thus, there were no positioning results. Based on the sequential search principle, the



FIGURE 6 Measured area.

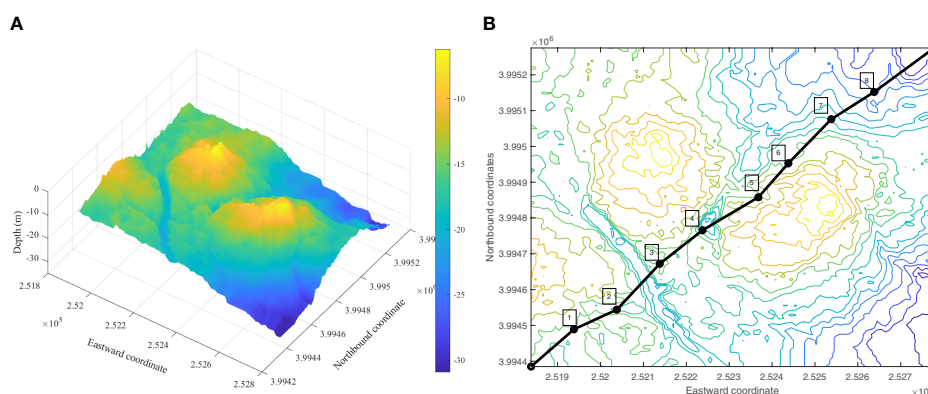


FIGURE 7 DTM (A: 3D digital terrain B: Contour map).

TABLE 3 Terrain entropy in matching area.

Matching area	Terrain entropy
1	2.96
2	2.39
3	2.24
4	1.55
5	2.19
6	3.22
7	3.95
8	4.57

positioning accuracy of the MLE-based method does not worsen with an increase in the IPE; however, it is affected by the richness of the terrain characteristics.

Simulation 2. For an IPE of 15 m, different sizes of the real-time terrain were selected; the simulation results are shown in Figures 10, 11. As the amount of real-time terrain data increased, the positioning error of the MRF-based method decreased. This is because an increase in the amount of data increases the range of the real-time terrain, as well as the overlap ratio between the real-time terrain and the local priori DTM, which can result in a more similar neighborhood distribution. In comparison, when the amount of real-time terrain data was relatively small, the positioning error of the MLE-based method decreased as the amount of data increased. Because of the “error averaging” effect, the positioning error cannot always be reduced as the amount of data increases continuously.

The above simulation and analysis show that the proposed method is affected by the amount of real-time terrain and IPEs. When the IPEs are small, the positioning accuracy of the proposed method is high. However, as the IPEs increase, the positioning accuracy decreases sharply. Therefore, to obtain higher positioning accuracy, smaller IPEs and larger amounts of real-time terrain data

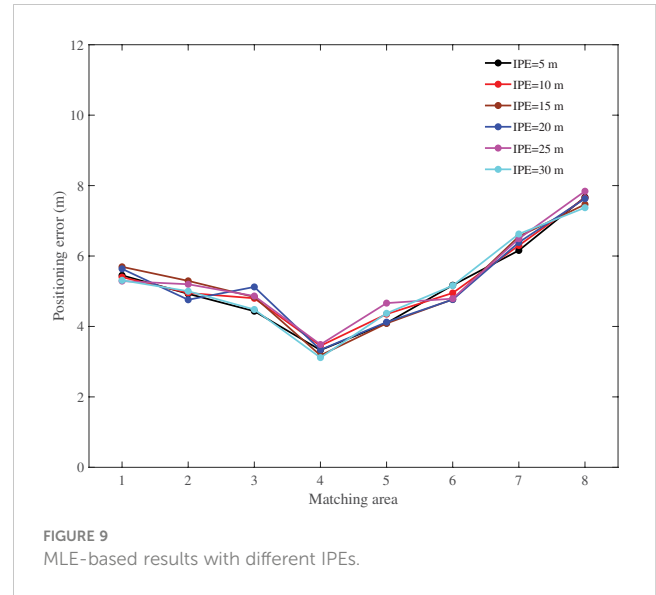


FIGURE 9 MLE-based results with different IPEs.

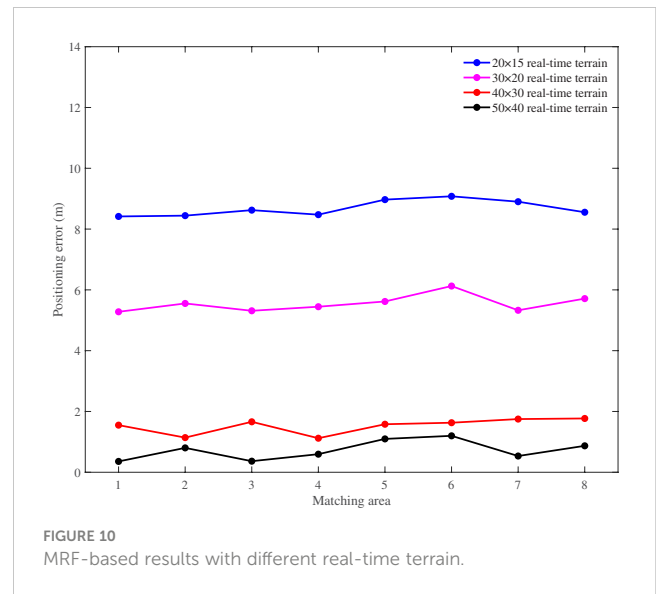


FIGURE 10 MRF-based results with different real-time terrain.

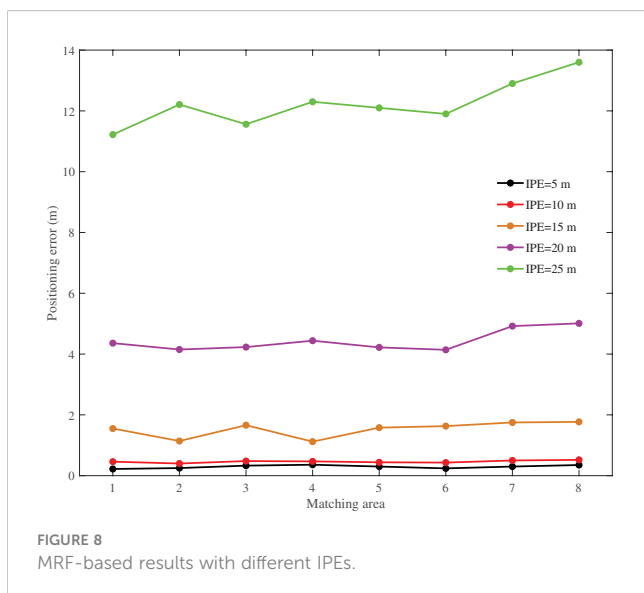


FIGURE 8 MRF-based results with different IPEs.

are required. In an actual scenario, owing to the cumulative error of the INS, small IPEs are essentially non-existent. Thus, rough matching positioning is required before the implementation of the proposed algorithm. As a classic terrain correlation method, the mean square difference (MSD) method (Feng, 2004) has the advantages of easy implementation and good real-time performance, and can be used for rough matching positioning.

Simulation 3. For an IPE of 30 m, the size of the real-time terrain was 50×40; the simulation results are shown in Figure 12.

As shown in Figure 12, the positioning accuracy of the MSD-based method is affected by the richness of the terrain characteristics; the positioning errors ranged between 8 and 16 m. After the precise positioning based on the MRF method, the positioning errors were less than 2 m. Simulation 2 showed that the positioning results diverged when the IPE reached 30 m. Thus, rough matching positioning is effective. As the covariance calculation in the MLE-based method was not performed in the

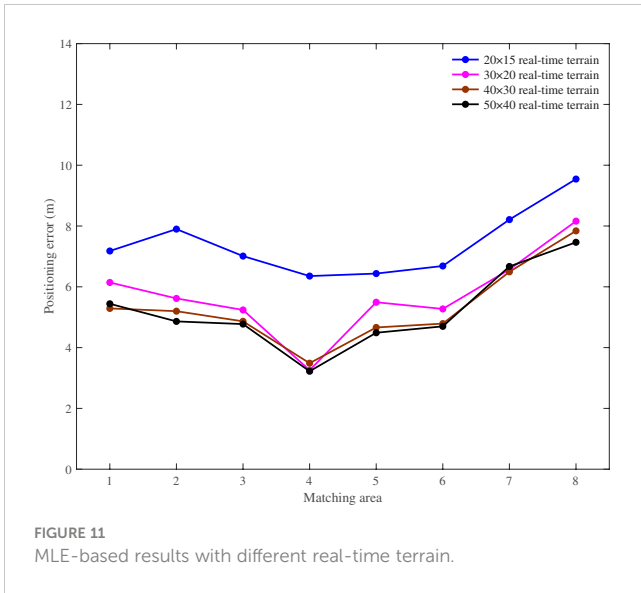


FIGURE 11 MLE-based results with different real-time terrain.

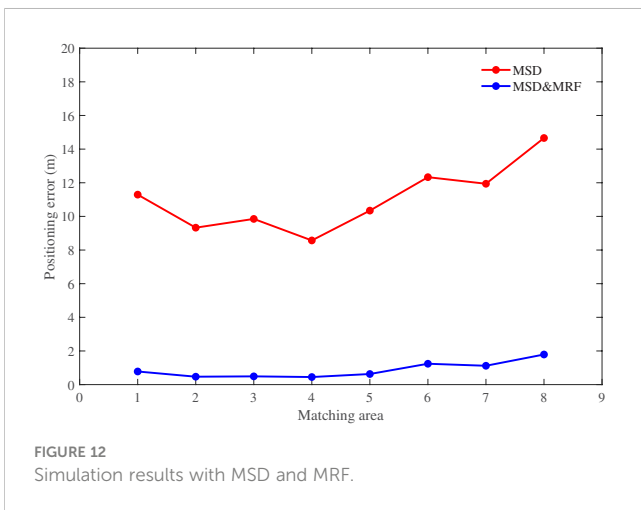


FIGURE 12 Simulation results with MSD and MRF.

MSD-based method, the MSD-based method exhibited good real-time performance. In simulation 3, the average positioning time of MSD-based method was less than 0.1 s, and the MLE-based method required about 0.4 s in the same simulation conditions. Thus, the MSD-based method can be used for approximately matching positioning.

4.4 Playback simulation test

The playback simulation implied that the sensor and environmental data were obtained from the sea trials. Based on the acquisition state in the sea trials, the data were read in real-time during the simulation. Because the data were obtained from sea trials, the playback simulation could simulate an actual marine environment; thus, the applicability of the proposed method was verified. The reference navigation data were independent dead-

reckoning data with a low-precision DVL that were not corrected using RTK. The playback simulation results are shown in Figure 13.

In the simulation, the UUV navigation information was provided by a reference navigation system. When the UUV navigated through the matching area, the terrain-matching navigation system was activated, and the positioning results were used to correct the cumulative errors of the reference navigation system. As shown in Figure 12, after rough matching positioning based on the MSD method, the positioning error was maintained within 15 m, which effectively reduced the initial positioning error for the MRF calculation. After the precise positioning based on the MRF method, the positioning error was less than 2 m in each matching area. Thus, the proposed method can effectively correct the cumulative error of a reference navigation system that can be used for underwater navigation.

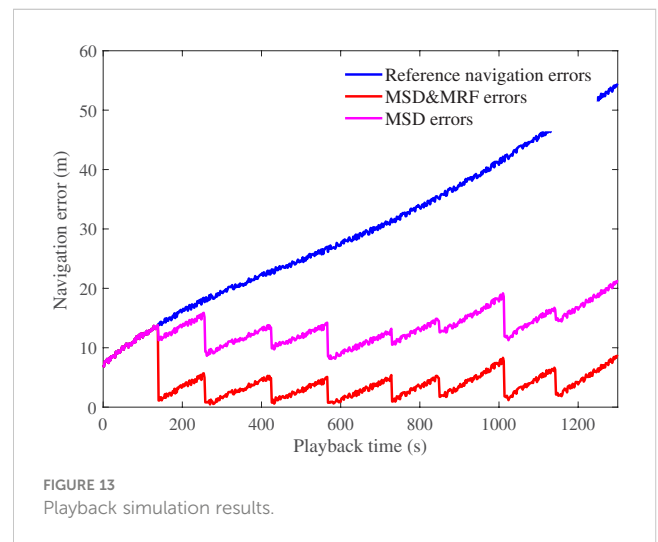


FIGURE 13 Playback simulation results.

5 Conclusions

In this study, an MRF-based UTPM model that achieves high positioning accuracy with small IPEs was developed. The following conclusions were drawn.

1. The proposed method focuses on the strong correlation between terrain data, which can be used to obtain good terrain adaptability.
2. The positioning error of the MRF-based method decreases with an increase in the amount of real-time terrain data. Thus, as much real-time terrain data as possible are required without affecting the real-time performance.
3. The main disadvantage of the MRF-based method is that the initial positioning deviation cannot be extremely large; otherwise, the matching accuracy decreases significantly. Thus, rough matching positioning is required before the implementation of the proposed algorithm.

Data availability statement

The original contributions presented in the study are included in the article/supplementary material. Further inquiries can be directed to the corresponding authors.

Author contributions

PC, TM and LZ contributed to conception and design of this research. XC carried out the database and figures processing. PC and XC performed the MATLAB/Simulink results analysis. PC, YL and TM wrote the first draft of the manuscript. YL revised the final manuscript. All authors contributed to the article and approved the submitted version.

Funding

This research was funded by the Key Research and Development Program of Shanxi Province (202202020101001), the National Natural Science Foundation of China (51909245,

62003314, 51279221), the Fundamental Research Program of Shanxi Province (202103021224187, 20210302124010, 20210302123050), and the Postgraduate Science and Technology Project of NUC (20221876).

Conflict of interest

The authors declare that the research was conducted in the absence of any commercial or financial relationships that could be construed as a potential conflict of interest.

Publisher's note

All claims expressed in this article are solely those of the authors and do not necessarily represent those of their affiliated organizations, or those of the publisher, the editors and the reviewers. Any product that may be evaluated in this article, or claim that may be made by its manufacturer, is not guaranteed or endorsed by the publisher.

References

- Arashloo, S. R., and Kittler, J. (2011). Energy normalization for pose-invariant face recognition based on MRF model image matching. *IEEE Trans. Pattern Anal. Mach. Intell.* 33 (6), 1274–1280. doi: 10.1109/TPAMI.2010.209
- Bergman, N., and Ljung, L. (1997). Point-mass filter and Cramer-rao bound for terrain-aided navigation (San Diego, California USA, in Proceedings of the 36th IEEE Conference on Decision and Control). 565–570. doi: 10.1109/CDC.1997.650690
- Chen, P. Y., Chen, X. L., Shen, J., and Ma, T. (2021). Single ping filtering of multi-beam sounding data based on alpha shapes. *Mar. Technol. Soc. J.* 55 (1), 106–114. doi: 10.4031/MTSJ.55.1.9
- Chen, P. Y., Li, Y., Su, Y. M., Chen, X. L., and Jiang, Y. Q. (2015a). Underwater terrain positioning method based on least squares estimation for AUV. *China Ocean Eng.* 29 (6), 859–874. doi: 10.1007/s13344-015-0060-9
- Chen, P. Y., Li, Y., Shen, P., Wang, R. P., and Jiang, Y. Q. (2015b). "Comparison and analysis of gridding methods of multi-beam echo sounder," in *Proceedings of the 27th Chinese Control and Decision Conference*. 2594–2597.
- Chen, X. L., Pang, Y. J., Li, Y., and Chen, P. Y. (2012). Underwater terrain matching positioning method based on MLE for AUV. *Robot* 34 (5), 559–565. doi: 10.3724/SP.J.1218.2012.00559
- Chen, P. Y., Zhang, P. F., Ma, T., Shen, P., Li, L., Wang, P. R., et al. (2019a). Underwater terrain positioning method using maximum a posteriori estimation and PCNN model. *J. Navig.* 72 (5), 1233–1253. doi: 10.1017/S0373463319000067
- Chen, P. Y., Zhang, P. F., Chang, J. L., and Shen, P. (2019b). Fast extraction of local underwater terrain features for underwater terrain-aided navigation. *J. Mar. Sci. Appl.* 18 (3), 334–342. doi: 10.1007/s11804-019-00086-6
- Feng, Q. T. (2004). *The research on new terrain elevation matching approaches and their applicability* (Changsha: National University of Defense Technology).
- Geman, S., and Geman, D. (1984). Stochastic relaxation, Gibbs distributions, and the Bayesian restoration of images. *IEEE Transactions on Pattern Analysis and Machine Intelligence*. PAMI-6 (6), 721–741. doi: 10.1109/TPAMI.1984.4767596
- GeoAcoustics Limited (2007). *GeoSwath plus operation manual* (UK: GeoAcoustics Limited).
- Hagen, O. K., Anonsen, K. B., and Saevo, T. O. (2012). Low-altitude terrain navigation for underwater vehicles integration of an interferometric side scan sonar improves terrain navigation in low-altitude scenarios. *Sea Technol.* 53 (6), 10–13.
- Huang, Y. L., Zhang, Y. G., and Zhao, Y. X. (2019). Review of autonomous undersea vehicle navigation methods. *J. Unmanned Veh. Syst.* 27 (3), 232–253. doi: 10.11993/j.issn.2096-3920.2019.03.002
- Jalving, B., Mandt, M., Hagen, O. K., and Phnern, F. (2004). *Terrain referenced navigation of AUVs and submarines using multibeam echo sounders* (Nice, France: Proceedings of UDT European), 1–10.
- Jiang, Y. Q., Ma, D., Li, Z. H., Li, Y., Ma, T., Su, X. F., et al. (2022). Cooperative terrain matching navigation of double autonomous underwater vehicles under the Arctic ice. *J. Harbin Eng. Univ.* 43 (8), 1091–1095. doi: 10.11990/jheu.202106022
- Li, P. J., Shen, G. L., Zhang, X. F., Wu, J. Q., and Xu, B. C. (2018). Underwater terrain-aided navigation system based on combination matching algorithm. *ISA Trans.* 78, 80–87. doi: 10.1016/j.isatra.2017.12.018
- Ma, T. (2019). *AUV bathymetric simultaneous localization and mapping*, [Ph.D thesis] (Harbin: Harbin Engineering University).
- Ma, T., Li, Y., Zhao, Y. X., Jiang, Y. Q., Cong, Z., Zhang, Q., et al. (2020). An AUV localization and path planning algorithm for terrain-aided navigation. *ISA Trans.* 103, 215–227. doi: 10.1016/j.isatra.2020.04.007
- Matthies, L., and Okutomi, M. (1990). A Bayesian foundation for active stereo vision. (1989, Philadelphia, PA, United States, in *Proceedings of 1989 Symposium on Visual Communications, Image Processing, and Intelligent Robotics Systems*) 1198, 62–74. doi: 10.1117/12.969965
- Nygren, I. (2005). *Terrain navigation for underwater vehicles* (Stockholm: Royal Institute of Technology).
- Peng, D. D., Zhou, T., Li, H. S., and Zhang, W. Y. (2016). Terrain aided navigation for underwater vehicles using maximum likelihood method. (Harbin, China, in *Proceedings of 2016 IEEE/OES China Ocean Acoustics Symposium*). 1–6. doi: 10.1109/COA.2016.7535750
- Salavasidis, G., Munafò, A., Harris, C. A., Prampart, T., Templeton, R., Smart, M., et al. (2019). Terrain-aided navigation for long-endurance and deep-rated autonomous underwater vehicles. *J. Field Robot.* 36 (2), 447–474. doi: 10.1002/rob.21832
- Salavasidis, G., Munafò, A., McPhail, S. D., Harris, C. A., Fenucci, D., Pebody, M., et al. (2021). Terrain-aided navigation with coarse maps—toward an arctic crossing with an AUV. *IEEE J. Ocean. Eng.* 46 (4), 1192–1212. doi: 10.1109/OJE.2021.3085941
- Shekhovtsov, A., Kovtun, I., and Hlavac, V. (2008). Efficient MRF deformation model for non-rigid image matching. *Comput. Vis. Image Underst.* 112, 91–99. doi: 10.1016/j.cviu.2008.06.006
- Teixeira, F. C., Quintas, J., Maurya, P., and Pascoal, A. (2017). Robust particle filter formulations with application to terrain-aided navigation. *Int. J. Adapt. Control Signal Process.* 31 (4), 608–651. doi: 10.1002/acs.2692
- Wang, H., Yan, L., Qian, X., and Zhu, M. (2007). Integration terrain match algorithm based on terrain entropy and terrain variance entropy. *comput. Technol. Dev.* 17 (9), 25–27. doi: 10.3969/j.issn.1673-629X.2007.09.008
- Xu, B. C., and Chen, Z. (2005). Novel scene matching algorithm based on Markov random field. *Opt. Tech.* 31 (60), 849–853. doi: 10.1081/CEH-200044273
- Yao, Y. B., Hu, M. X., and Xu, C. L. (2016). Positioning accuracy analysis of GPS/BDS/GLONASS network RTK based on DREAMNET. *Acta Geod. Cartogr. Sin.* 45 (9), 1009–1018. doi: 10.11947/j.AGCS.2016.20160133

Zhang, T. W., Han, G. J., Lin, C., Guizani, M., Li, H. B., and Shu, L. (2020a). Integration of communication, positioning, navigation and timing for deep-sea vehicles. *IEEE Netw.* 34 (2), 121–127. doi: 10.1109/MNET.001.1900294

Zhang, T. W., Han, G. J., Guizani, M., Yan, L., and Shu, L. (2020b). Peak extraction passive source localization using a single hydrophone in shallow water. *IEEE Trans. Veh. Technol.* 69 (3), 3412–3423. doi: 10.1109/TVT.2020.2968500

Zhao, L., Gao, N., Huang, B. Q., Wang, Q. Y., and Zhou, J. H. (2015). A novel terrain-aided navigation algorithm combined with the TERCOM algorithm and particle filter. *IEEE Sens. J.* 15 (2), 1124–1131. doi: 10.1109/JSEN.2014.2360916

Zhou, Y. J., and Zheng, T. (2012). Sea Bottom terrain aided navigation based on the kalman filter. *Ship Electronic Eng.* 32 (4), 54–56. doi: 10.3969/j.issn.1627-9730.2012.04.019